

# An effective excess charge model to describe hysteresis effects on streaming potential

M. Soldi<sup>1\*</sup>, L. Guarracino<sup>1</sup> and D. Jougnot<sup>2</sup>

<sup>1</sup>Facultad de Ciencias Astronómicas y Geofísicas, Universidad Nacional de La Plata, Consejo Nacional de Investigaciones Científicas y Técnicas, La Plata, Argentina

<sup>2</sup>Sorbonne Université, CNRS, EPHE, UMR 7619 METIS, Paris, France

\*E-mail: msoldi@fcaglp.unlp.edu.ar

This paper has been published in Journal of Hydrology:  
Soldi, M., Guarracino, L. and Jougnot, D. An effective excess charge model to describe hysteresis effects on streaming potential. Journal of Hydrology (2020).  
<https://doi.org/10.1016/j.jhydrol.2020.124949>

## Abstract

Streaming potentials are produced by the coupling between the water flow and the electrical current generated by the drag of electrical charges within the pore water of the media. This electrokinetic coupling is strongly influenced by the hydraulic properties that control groundwater flow (permeability, saturation and pressure head). Under unsaturated conditions, hydrogeologic studies have widely established that the relationships of permeability and saturation with pressure head are different for drainage and imbibition experiments. The hysteresis phenomenon present on these properties produces a hysteretic behaviour on the streaming potential which has been recently observed in experimental data. Hysteresis can be explained by the presence of irregularities in the pore geometry of the media which affects the water flow and, therefore, the excess charge density that is effectively dragged by the flow. In this study, we present a physically-based analytical model to describe the hysteresis phenomenon in the estimates of the effective excess charge density. Under the assumptions of a porous medium represented by a bundle of tortuous capillary tubes with throats and a fractal pore size distribution, hysteretic curves are obtained for the effective excess charge density as a function of pressure head using a flux averaging technique. These analytical expressions are closed-form and depend on the medium petrophysical and chemical properties. The predictions of the proposed model are consistent with laboratory data from drainage-imbibition experiments. These results open up exciting possibilities for studies involving water movement and processes in the vadose zone.

Keywords: Hydrogeophysics, Streaming Potential, Hysteresis, Vadose zone

## 1 Introduction

Understanding and monitoring water movement in the subsurface is important to characterize the processes occurring in the earth critical zone. Indeed, water plays crucial roles

27 in supporting terrestrial life, shaping and interacting with that zone (Fan et al., 2019).  
28 Among the different electrical methods used to study groundwater, the self-potential (SP)  
29 method has proven to be the most appropriate for characterizing water flow since its sen-  
30 sitivity to water flux direction and velocity. This passive geophysical method relies on the  
31 measurement of electrical potential differences (i.e., the electrical field) using two or more  
32 non-polarizable electrodes (e.g., Petiau, 2000) and a high impedance voltmeter. It can be  
33 employed performing snapshots or monitoring of profiles, maps (e.g., Jardani et al., 2006),  
34 or vertically distributed in the ground (e.g., Doussan et al., 2002; Jougnot et al., 2015).  
35 The SP method was effectively used to monitor pumping and recovery tests (e.g., Rizzo  
36 et al., 2004; Straface et al., 2007; Malama et al., 2009b; Soueid Ahmed et al., 2014), and  
37 also environmental studies such as CO<sub>2</sub> flooding (e.g., Büsing et al., 2017), contaminant  
38 fluxes (e.g., Linde and Revil, 2007) and root-water uptake (e.g., Voytek et al., 2019). The  
39 recorded SP signals are a superposition of different contributions related to electrokinetic,  
40 redox and diffusion phenomena. In this study, we focus on the electrokinetic (EK) contri-  
41 bution which is predominant in hydrological studies as it is generated from the water flow  
42 in porous media. The origin of the EK contribution to the SP signal lies in the presence  
43 of an electrical double layer (EDL) in the pore water created by the electrical charges that  
44 are generally found at the mineral surface (Stern, 1924). The EDL contains an excess  
45 of charge that counterbalances the charge deficiency of the mineral surface. This excess  
46 of charge is distributed in two layers within the EDL (see Fig. 1). Close to the mineral  
47 surface is where most of the excess charge is distributed in a fixed layer with a very limited  
48 thickness called the Stern layer, and the rest of the remaining fraction is contained and  
49 flows in the diffuse layer (or Gouy-Chapman layer). The limit between these two layers  
50 can be approximated by the shear plane which is characterized by an electrical potential  
51 called  $\zeta$ -potential (e.g. Hunter, 1981).

52 Flow and transport in partially saturated soils are significantly influenced by the hys-  
53 teresis phenomenon present in the hydraulic properties of the porous media (e.g., Topp,  
54 1971; Mualem, 1977; Jury et al., 1991; Pham et al., 2005). Recent studies have shown the  
55 importance of the hysteresis phenomenon regarding the SP signal. Doussan et al. (2002)  
56 measured SP signals during rainfall events and observed differences in the water flux esti-  
57 mates when considering drainage and imbibition phases. Mainault et al. (2008) measured  
58 variations of the SP signal during periodic pumping tests performed at a test site located  
59 near a freshwater reservoir. Whereas they observed a correlation between the pumping  
60 and the SP signal, a phase-lag was found between the SP and pressure head measurements  
61 which they related to drainage-imbibition cycles. Revil et al. (2008) performed numerical  
62 experiments with harmonic pumping tests in an unconfined aquifer. They observed that  
63 the experiment accounting for a hysteretic flow model could explain the SP variations  
64 found by Mainault et al. (2008). In order to extract valuable information from pumping  
65 tests using SP data, it is necessary to rely on accurate models. For example, Malama  
66 et al. (2009a) developed mathematical solutions for the SP signals associated to pumping  
67 test in unconfined aquifers. Later, Soueid Ahmed et al. (2016) developed a hydraulic  
68 tomography approach for an aquifer in transient conditions from SP and hydraulic head  
69 data. In this work the authors mention the importance of the hysteresis of the hydraulic

70 properties in the SP signals. Haas and Revil (2009) measured SP signals resulting from  
71 Haines jumps during the drainage and imbibition of a sandbox and observed that in each  
72 case the electrical signature was different. The drainage experiment exhibited a larger  
73 amount of electrical bursts in the SP signals than the imbibition experiment. Jougnot  
74 et al. (2012) developed two flux averaging approaches to estimate the EK contribution  
75 to the SP signal by considering that the pore distribution of the media can be derived  
76 from the water retention function or from the relative permeability function. They tested  
77 both approaches against an unsaturated vertical hydraulic flux due to rainfall events from  
78 Doussan et al. (2002). While their model predicted well the first rainfall, the follow-  
79 ing events presented an increasing discrepancy. They considered that hysteretic effects  
80 due to drainage-imbibition cycles of the soil may explain that observation. Allègre et al.  
81 (2014) performed a study of the SP response to drainage and imbibition experiments in  
82 a sand column and observed that the SP signal presented a hysteretic behaviour with  
83 respect to pressure head. Later, Zhang et al. (2017) presented a methodology to deter-  
84 mine a relationship between the streaming potential coupling coefficient and saturation  
85 for unsaturated flow during drainage and imbibition experiments.

86 In order to study SP phenomena, two approaches have been developed over the years  
87 to model the streaming current generation. On the one side, the Helmholtz-Smoluchowski  
88 coupling coefficient approach focuses on the evolution with varying water saturation of  
89 the coupling coefficient which relates an electrical potential and a hydraulic pressure head  
90 differences (Guichet et al., 2003; Jackson, 2010; Allègre et al., 2014). This approach  
91 neglects electrical surface conductivity on the mineral surface, nevertheless alternative  
92 formulas have been proposed by several researchers in order to account this effect (e.g.,  
93 Morgan et al., 1989; Revil et al., 1999; Glover and Déry, 2010). On the other side,  
94 the second approach is more recent and focuses on the excess charge that is effectively  
95 dragged by the water flux in the pore space (e.g., Kormiltsev et al., 1998; Linde et al.,  
96 2007; Revil et al., 2007; Jougnot et al., 2012; Revil, 2017; Guarracino and Jougnot, 2018;  
97 Jougnot et al., 2020). In this approach, the streaming current can be expressed as the  
98 product between the effective excess charge density and the water flux velocity. While  
99 both approaches describe the same physics, the difference lies in which parameter is used  
100 to describe the electrokinetic coupling between the streaming potential and the water  
101 flux. An interesting point of the second approach is that it allows the decomposition  
102 of the coupling coefficient in three components: the relative permeability, the electrical  
103 conductivity and the effective excess charge density. Whereas all of these components  
104 depend on the water saturation, the behaviour of each one is different. The behaviour of  
105 the first two components under unsaturated conditions has been studied for decades (e.g.,  
106 Archie et al., 1942; Waxman and Smits, 1968; Mualem, 1986; Lenhard and Parker, 1987),  
107 nevertheless, how the effective excess charge density varies with saturation is a current  
108 theme of study that requires more development (e.g., Jougnot et al., 2012; Revil, 2017;  
109 Thanh et al., 2018; Soldi et al., 2019).

110 Based on the coupling coefficient approach, Revil et al. (2007) proposed the first  
111 model to describe the hysteresis phenomenon in the streaming potential. They considered  
112 two sets of van Genuchten parameters (one for the drainage and one for the imbibition

113 experiments) in order to model this phenomenon in the variation of the coupling coefficient  
 114 with the saturation. Later, Jougnot and Linde (2013) also employed this approach to  
 115 reproduce the SP signal during drainage and imbibition experiments. In this study, we  
 116 consider the framework developed by Sill (1983) and focus on the effective excess charge  
 117 approach proposed by Kormiltsev et al. (1998) and Revil et al. (2007) where the EK signal  
 118 can be directly related to the water flux velocity:

$$\nabla \cdot (\sigma \nabla \varphi) = \nabla \cdot (\hat{Q}_v \mathbf{u}) \quad (1)$$

119 being  $\sigma$  ( $\text{S m}^{-1}$ ) the bulk electrical conductivity,  $\varphi$  (V) the electrical potential,  $\hat{Q}_v$  ( $\text{C}$   
 120  $\text{m}^{-3}$ ) the excess charge effectively dragged by the water flux and  $\mathbf{u}$  ( $\text{m s}^{-1}$ ) the water flux  
 121 which follows Buckingham-Darcy's law (Buckingham, 1907; Darcy, 1856).

122 In order to describe the water flow at the representative elementary volume (REV)  
 123 scale, capillary tube models have proven to be useful for characterizing the porous media  
 124 by considering different shapes and pore size distributions (e.g., Jerauld and Salter, 1990;  
 125 Xu and Torres-Verdín, 2013; Wang et al., 2015). Recently, these models have provided  
 126 valuable insight in the study of, for example, mineral dissolution (e.g., Guarracino et al.,  
 127 2014), electrical conductivity (e.g., Thanh et al., 2019), saturation hysteretic effects on  
 128 seismic signatures (e.g., Solazzi et al., 2019) and streaming potential phenomenon (e.g.,  
 129 Jackson, 2008, 2010; Linde, 2009; Jougnot et al., 2012, 2015; Thanh et al., 2018; Guar-  
 130 racino and Jougnot, 2018). In this study, we derive an analytical model to describe the  
 131 hysteresis phenomenon in the effective excess charge density under partially saturated  
 132 conditions. For this purpose, we base our approach on the capillary tube model proposed  
 133 by Soldi et al. (2017) that only describes the hydraulic properties of a partially satu-  
 134 rated porous media. The key feature of this model is that it includes hysteresis effects  
 135 in the water flow properties by considering irregularities in the structure of the tubes.  
 136 The pore geometry of this model is represented by a bundle of capillary tubes with peri-  
 137 odic reductions in the pore radius (constrictivities or "ink-bottle") and a fractal pore size  
 138 distribution. This pore geometry causes a different saturation pattern during drainage  
 139 and imbibition that can be used to model hysteresis in macroscopic hydraulic properties.  
 140 Nonetheless, other effects could also contribute or explain the presence of the hysteresis  
 141 phenomenon in porous media such as contact angle effects, entrapped air and pore network  
 142 connectivity (e.g., Jury et al., 1991; Klausner, 1991; Vogel and Roth, 2001). Therefore, as-  
 143 suming this pore geometry, the excess charge effectively dragged by the water flow is first  
 144 calculated for one single constrictive capillary tube (i.e. referred to as microscale) and is  
 145 then upscaled to the bundle of capillary tubes (i.e. the REV scale) using a flux-averaging  
 146 technique. Closed-form analytical expressions for the effective excess charge density are  
 147 obtained as a function of pressure head. The periodic constrictivities of the pores allow to  
 148 introduce the hysteresis phenomenon in the model's expressions in a simple form due to  
 149 the strong control of those irregularities over the water flow. The proposed model is con-  
 150 sistent with the previous model of Soldi et al. (2019) for non-constrictive capillary tubes,  
 151 and with experimental laboratory data from drainage and imbibition cycles. Moreover,  
 152 the relationship between the effective excess charge density and the coupling coefficient  
 153 allowed us to estimate this last coefficient for different soil textures and also observed its

154 hysteretic behaviour when expressed as a function of pressure head.

## 155 2 Hysteretic analytical model

156 In the present section, we derive an analytical closed form expression for the effective  
 157 excess charge density. The proposed model is based on the macroscopic description of the  
 158 effective excess charge density that is dragged by the water flow in the porous media and  
 159 that can be obtained from the upscaling of pore size flow and electrokinetic phenomena.  
 160 First, we present the pore geometry, the pore size distribution law and the hysteretic  
 161 hydraulic properties obtained at macroscopic scale from Soldi et al. (2017). Then, we  
 162 derive the electrokinetic properties, for a single pore and for a REV of porous media, and  
 163 we obtain effective excess charge density curves for drainage and imbibition as functions  
 164 of pressure head.

165

166 At microscopic scale, we consider that the pore structure of the media is represented by  
 167 tortuous capillary tubes with varying aperture. Each pore is conceptualized as a circular  
 168 tube of radius  $R$  (m) and length  $l$  (m) with periodically pore throats  $aR$  (as illustrated  
 169 in Fig. 1) where  $a$  is the radial factor that represents the ratio in which the radius is  
 170 reduced ( $0 \leq a \leq 1$ , dimensionless). Then, under the assumption that the pore geometry  
 171 has a wavelength  $\lambda$  and that the length of the tube contains an integer number  $M$  of  
 172 wavelengths, the pore radius along the tube can be expressed as (Soldi et al., 2017):

$$r(x) = \begin{cases} aR & \text{if } x \in [0 + \lambda n, \lambda c + \lambda n) \\ R & \text{if } x \in [\lambda c + \lambda n, \lambda + \lambda n), \end{cases} \quad (2)$$

173 where  $c$  is the length factor ( $0 \leq c \leq 1$ , dimensionless) that represents the segment of  $\lambda$   
 174 with pore throat and  $n = 0, 1, \dots, M - 1$ .

175

176 At macroscopic scale, we consider as a representative elementary volume (REV) a  
 177 cylinder of radius  $R_{REV}$  (m) and length  $L$  (m). The porous space of the REV is represented  
 178 by a bundle of capillary tubes whose radii vary between a minimum  $R_{min}$  (m) and a  
 179 maximum  $R_{max}$  (m) pore radius value.

180 The number of pores whose radii are greater than or equal to  $R$  is assumed to follow  
 181 a fractal law given by (Tyler and Wheatcraft, 1990; Yu et al., 2003; Soldi et al., 2017,  
 182 2019):

$$N(R) = \left( \frac{R_{REV}}{R} \right)^D, \quad (3)$$

183 where  $D$  is the pore fractal dimension ( $1 < D < 2$ , dimensionless) and  $0 < R_{min} \leq R \leq$   
 184  $R_{max} < R_{REV}$ .

185 Differentiating the cumulative pore size distribution given by Eq. (3) with respect to  
 186  $-R$ , we obtain the number of pores whose radii are within the infinitesimal range  $R$  and  
 187  $R + dR$ :

$$dN(R) = DR_{REV}^D R^{-D-1} dR. \quad (4)$$

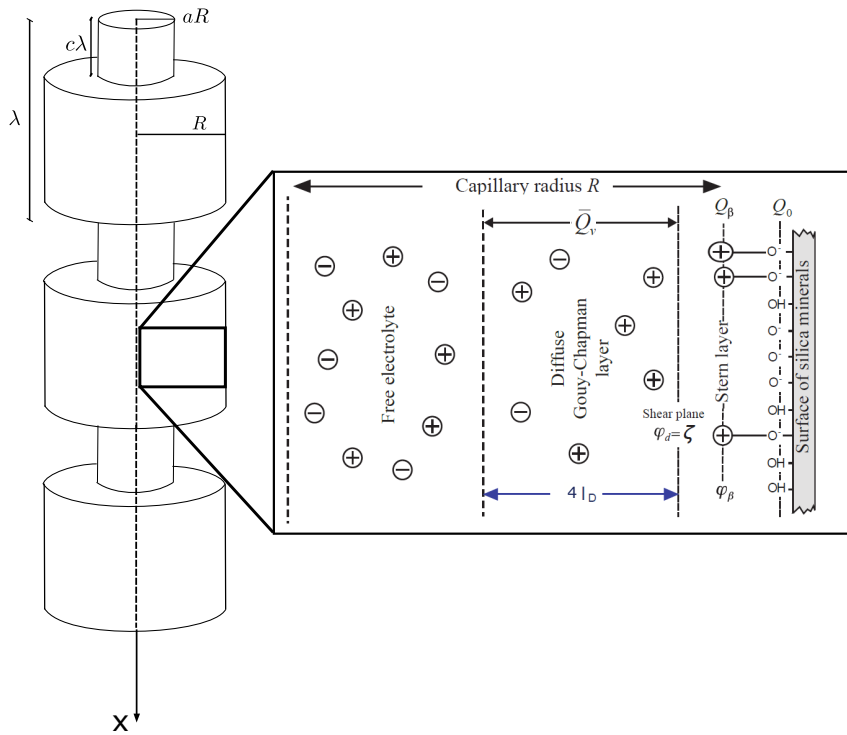


Figure 1: Schemes of the pore geometry of a single capillary tube with periodic pore throats (on the left) and of the electrical layers within the capillary (on the right).

## 2.1 Hydraulic properties

In this Section, we present the expressions of the REV's porosity, and the effective saturation and relative permeability curves as function of the pressure head from Soldi et al. (2017). These curves are different for drainage and imbibition tests due to the presence of the pore throats.

The porosity  $\phi$  of the REV can be computed from its definition as the ratio of the pore volume to the total volume of the REV. For the proposed geometry, the expression of  $\phi$  yields:

$$\phi = \frac{f_v(a, c)D\tau}{R_{REV}^{(2-D)}(2-D)} [R_{max}^{2-D} - R_{min}^{2-D}], \quad (5)$$

where  $\tau = l/L$  (dimensionless) is the hydraulic tortuosity of the pores and

$$f_v(a, c) = a^2c + 1 - c. \quad (6)$$

This factor  $f_v$  varies between 0 and 1 (see Fig. 2a from Soldi et al., 2017) and quantifies the reduction in the pore volume due to the presence of the pore throats.

To obtain the main drying effective saturation curve, we consider that the REV is initially fully saturated and a pressure head  $h$  is applied in order to drain it. For a tube with constant radius, the pressure head  $h$  (m) can be related to the radius of the pore  $R_h$  by (Bear, 1998):

$$h = \frac{2T_s \cos(\beta)}{\rho g R_h}, \quad (7)$$

where  $T_s$  (N m<sup>-1</sup>) is the surface tension of the water,  $\beta$  the contact angle,  $\rho$  (kg m<sup>-3</sup>) the water density and  $g$  (m s<sup>-2</sup>) the gravity acceleration. For a drainage experiment, it is then reasonable to consider that the pores with radii between  $R_{min}$  and  $R_h/a$  will remain fully saturated since we assume that a pore is fully desaturated if its pore throat radius  $aR$  is greater than the radius  $R_h$  (Eq. (7)). Therefore, the main drying effective saturation curve  $S_e^d$  can be expressed as (Soldi et al., 2017):

$$S_e^d(h) = \begin{cases} 1 & \text{if } h \leq \frac{h_{min}}{a} \\ \frac{(ha)^{D-2} - h_{max}^{D-2}}{h_{min}^{D-2} - h_{max}^{D-2}} & \text{if } \frac{h_{min}}{a} < h < \frac{h_{max}}{a}, \\ 0 & \text{if } h \geq \frac{h_{max}}{a} \end{cases} \quad (8)$$

where

$$h_{min} = \frac{2T_s \cos(\beta)}{\rho g R_{max}} \quad h_{max} = \frac{2T_s \cos(\beta)}{\rho g R_{min}}, \quad (9)$$

$h_{min}$  and  $h_{max}$  are the minimum and maximum pressure heads defined by  $R_{max}$  and  $R_{min}$ , respectively.

For an imbibition experiment, we consider that the REV is fully desaturated and it is flooded with a pressure head  $h$ . Then, the pores whose radii are between  $R_{min}$  and  $R_h$  will

214 be fully saturated and the main wetting effective saturation curve  $S_e^w$  can be computed  
 215 as (Soldi et al., 2017):

$$S_e^w(h) = \begin{cases} 1 & \text{if } h \leq h_{min} \\ \frac{h^{D-2} - h_{max}^{D-2}}{h_{min}^{D-2} - h_{max}^{D-2}} & \text{if } h_{min} < h < h_{max}. \\ 0 & \text{if } h \geq h_{max} \end{cases} \quad (10)$$

216 Recently, this saturation model has been effectively used to estimate the effect of hys-  
 217 teretic saturation fields on seismic signatures which are generally observed in laboratory  
 218 during drainage and imbibition experiments (Solazzi et al., 2019).

219

220 Similarly, considering the same hypotheses and the Buckingham-Darcy law for unsat-  
 221 urated water flow, Soldi et al. (2017) obtained the main drying relative permeability curve  
 222  $k_{rel}^d$  as a function of pressure head for a drainage experiment which is given by:

$$k_{rel}^d(h) = \begin{cases} 1 & \text{if } h \leq \frac{h_{min}}{a} \\ \frac{(ha)^{D-4} - h_{max}^{D-4}}{h_{min}^{D-4} - h_{max}^{D-4}} & \text{if } \frac{h_{min}}{a} < h < \frac{h_{max}}{a}, \\ 0 & \text{if } h \geq \frac{h_{max}}{a} \end{cases} \quad (11)$$

223 while for an imbibition experiment, the main wetting relative permeability curve  $k_{rel}^w$  can  
 224 be expressed as:

$$k_{rel}^w(h) = \begin{cases} 1 & \text{if } h \leq h_{min} \\ \frac{h^{D-4} - h_{max}^{D-4}}{h_{min}^{D-4} - h_{max}^{D-4}} & \text{if } h_{min} < h < h_{max}. \\ 0 & \text{if } h \geq h_{max} \end{cases} \quad (12)$$

225 Note that Eqs. (8), (10), (11) and (12) can be used to compute the main drying and  
 226 wetting curves of the hysteretic cycle observed in the effective saturation and relative  
 227 permeability. Scanning curves can be scaled from these main curves using different ap-  
 228 proaches for any intermediate state (e.g., Parker and Lenhard, 1987; Beliaev and Has-  
 229 sanizadeh, 2001). It is important to remark that relative permeability can be expressed  
 230 as a function of effective saturation which yields in a non-hystertic function (see Ec. (28)  
 231 from Soldi et al., 2017). This means that the relationship between these two variables  
 232  $k_{rel}(S_e)$  is unique for the drying and the wetting, and this result is consistent with ob-  
 233 served experimental data (e.g. Topp and Miller, 1966; Van Genuchten, 1980; Mualem,  
 234 1986).



## 2.2 Electrokinetic properties

In this section we derive expressions to estimate the electrokinetic phenomenon which results from a coupling between hydraulic and electrokinetic properties at pore scale. We consider that the capillary tubes are saturated by a binary symmetric 1:1 electrolyte (e.g., NaCl). Under the hypothesis of a thin double layer (the thickness of the electrical double layer is small compared to the pore radius), the effective excess charge density carried by the water flow in a single tube of constant radius  $R$  is given by (Guarracino and Jougnot, 2018):

$$\hat{Q}_v^R = \frac{8N_A e_0 C_w^0}{(R/l_D)^2} \left[ -\frac{2e_0\zeta}{k_B T} - \left( \frac{e_0\zeta}{3k_B T} \right)^3 \right], \quad (13)$$

where  $N_A$  ( $\text{mol}^{-1}$ ) is Avogadro's number,  $e_0$  (C) the elementary charge,  $C_w^0$  ( $\text{mol L}^{-1}$ ) the ionic concentration far from the mineral's surface,  $\zeta$  (V) the zeta potential,  $k_B$  ( $\text{J K}^{-1}$ ) the Boltzmann constant,  $T$  (K) the temperature and  $l_D$  (m) the Debye length which is defined by:

$$l_D = \sqrt{\frac{\varepsilon k_B T}{2N_A C_w^0 e_0^2}}, \quad (14)$$

being  $\varepsilon$  ( $\text{F m}^{-1}$ ) the pore water dielectric permittivity. Note that Eq. (13) is considered valid when the pore radius is greater than  $5l_D$  (see Guarracino and Jougnot, 2018; Jougnot et al., 2019).

By assuming the conservation of the electrical charges in the pore volume, the effective excess charge density carried by the water flux in a capillary tube with pore throats  $\hat{Q}_v^p$  ( $\text{C m}^{-3}$ ) can be expressed as:

$$\hat{Q}_v^p(R) = \frac{1}{V_p} \int_0^l \hat{Q}_v^r \pi r^2(x) dx = \frac{M}{V_p} \left[ \int_0^{\lambda c} \hat{Q}_v^{aR} \pi (aR)^2 dx + \int_{\lambda c}^{\lambda} \hat{Q}_v^R \pi R^2 dx \right] = \hat{Q}_v^R \frac{1}{f_v}, \quad (15)$$

where  $V_p = \pi R^2 l f_v$  is the volume of a single pore. Note that  $\hat{Q}_v^p$  depends inversely on the factor  $f_v$  which is a function of the pore geometry parameters,  $a$  and  $c$  (Eq. (6)). As mentioned in Section 2.1,  $f_v$  can vary between 0 and 1, and the inverse of this factor is then greater or equal to 1. Figure 2 shows the effect of the radial factor  $a$  on  $1/f_v$  for different constant values of the length factor  $c$  (0.1, 0.3 and 0.5). Despite of the fact that  $c$  can vary between 0 and 1, we considered values in the range of 0 to 0.5 for representing realistic pore geometries. It is interesting to observe that as the factor  $a$  decreases, the radius of the pore is reduced significantly producing a larger effect on the  $\hat{Q}_v^p$  values. Therefore, the pore throat plays a key role in the estimates of the effective excess charge density.

In order to derive the effective excess charge density  $\hat{Q}_v^{REV}$  carried by the water flow in the REV, we consider conditions of saturation similar to those used to compute the hydraulic properties (Section 2.1). For a drainage test, we assume that a pressure head  $h$  is applied to drain a fully saturated REV. Then, only the pores that remain fully saturated ( $R_{min} \leq R \leq R_h/a$ ) contribute to the volumetric water flow, and hence to the effective

268 excess charge density  $\hat{Q}_v^{REV,d}$  (C m<sup>-3</sup>). Considering a flux averaging technique, the total  
 269  $\hat{Q}_v^{REV,d}$  can be computed by integrating the individual contribution of each pore as:

$$\hat{Q}_v^{REV,d} = \frac{1}{v_D \pi R_{REV}^2} \int_{R_{min}}^{\frac{R_h}{a}} \hat{Q}_v^p(R) q_p(R) dN(R), \quad (16)$$

270 where  $v_D = \frac{\rho g}{\eta} k_{rel} k \frac{\Delta h}{L}$  (m s<sup>-1</sup>) is the Darcy's velocity and  $q_p(R)$  (m<sup>3</sup> s<sup>-1</sup>) the volumetric  
 271 flow rate of a pore with varying aperture given by (Soldi et al., 2017):

$$q_p(R) = \frac{\rho g}{\eta} \frac{\pi R^4}{8} f_k(a, c) \frac{\Delta h}{l}, \quad (17)$$

272 being

$$f_k(a, c) = \frac{a^4}{c + a^4(1 - c)} \quad (18)$$

273 the factor that quantifies the reduction in the volumetric water flow due to the pore  
 274 throats. This factor is dimensionless and varies between 0 and 1.

275 Substituting Eqs. (4), (15) and (17) in (16) and combining the resulting expression  
 276 with Eqs. (5) and (8) yields:

$$\hat{Q}_v^{REV,d} = N_A e_0 C_w^0 \left[ -\frac{2e_0\zeta}{k_B T} - \left( \frac{e_0\zeta}{3k_B T} \right)^3 \right] \frac{l_D^2}{\tau^2} \frac{f_k}{f_v^2} \frac{\phi}{k} \frac{S_e^d}{k_{rel}^d}. \quad (19)$$

277 Similarly, for an imbibition test, we consider that the REV is saturated with a pressure  
 278 head  $h$ . The pores with radius smaller than  $R_h$  will be fully saturated and thus contribute  
 279 to the water flow. Then, the effective excess charge density  $\hat{Q}_v^{REV,w}$  can be expressed as:

$$\hat{Q}_v^{REV,w} = N_A e_0 C_w^0 \left[ -\frac{2e_0\zeta}{k_B T} - \left( \frac{e_0\zeta}{3k_B T} \right)^3 \right] \frac{l_D^2}{\tau^2} \frac{f_k}{f_v^2} \frac{\phi}{k} \frac{S_e^w}{k_{rel}^w}. \quad (20)$$

280 Note that in the case of non-constrictive tubes,  $a = 1$  (or  $c = 0$ ) which yields to  $f_v = f_k =$   
 281 1, Eqs. (19) and (20) have the same analytical expression which is the equation obtained  
 282 by Soldi et al. (2019) for the effective excess charge density in tortuous straight tubes.

283 Equations (19) and (20) can be expressed as:

$$\hat{Q}_v^{REV,i} = \hat{Q}_v^{REV,sat} \hat{Q}_v^{REV,rel,i} \quad (21)$$

284 where the effective excess charge density for saturated conditions  $\hat{Q}_v^{REV,sat}$  (C m<sup>-3</sup>) is  
 285 given by:

$$\hat{Q}_v^{REV,sat} = N_A e_0 C_w^0 \left[ -\frac{2e_0\zeta}{k_B T} - \left( \frac{e_0\zeta}{3k_B T} \right)^3 \right] \frac{l_D^2}{\tau^2} \frac{f_k}{f_v^2} \frac{\phi}{k} \quad (22)$$

286 and the relative effective excess charge density  $\hat{Q}_v^{REV,rel}$  (dimensionless) by:

$$\hat{Q}_v^{REV,rel,i} = \frac{S_e^i}{k_{rel}^i} \quad (23)$$

287 being  $i = d, w$ . Note that the  $\hat{Q}_v^{REV,sat}$  factor is the same for both drainage and imbibition  
 288 experiments and depends on petrophysical and electro-chemical properties. However,  
 289 the  $\hat{Q}_v^{REV,rel,i}$  factor only depends on the hydraulic properties of the media which differ  
 290 between drainage and imbibition tests. Then, the hysteresis phenomenon in the effective  
 291 excess charge density is associated with the relative factor.

292 By inspection of Eq. (23), it can be noticed that when  $S_e$  approaches zero, both  
 293 terms of the quotient tend to zero for drainage (when  $h \rightarrow h_{max}/a$ ) and imbibition (when  
 294  $h \rightarrow h_{max}$ ). From Eqs. (8), (11), (10) and (12), we obtain the same asymptotic value for  
 295 drainage and imbibition:

$$\lim_{S_e \rightarrow 0} \hat{Q}_v^{REV,rel,i} = \lim_{h \rightarrow \frac{h_{max}}{a}} \frac{S_e^d(h)}{k_{rel}^d(h)} = \lim_{h \rightarrow h_{max}} \frac{S_e^w(h)}{k_{rel}^w(h)} = \frac{h_{min}^{D-4} - h_{max}^{D-4}}{h_{min}^{D-2} - h_{max}^{D-2}}. \quad (24)$$

296 This limit case represents the excess charge of the pores with smallest radius dragged by  
 297 the residual water saturation.

298 The main drying relative effective excess charge density curve  $\hat{Q}_v^{REV,rel,d}$  as a function  
 299 of the pressure head  $h$  can be obtained by substituting Eqs. (8) and (11) into Eq. (23):

$$\hat{Q}_v^{REV,rel,d}(h) = \begin{cases} 1 & \text{if } h \leq \frac{h_{min}}{a} \\ \frac{(ha)^{D-2} - h_{max}^{D-2}}{(ha)^{D-4} - h_{max}^{D-4}} \cdot \frac{h_{min}^{D-4} - h_{max}^{D-4}}{h_{min}^{D-2} - h_{max}^{D-2}} & \text{if } \frac{h_{min}}{a} < h < \frac{h_{max}}{a} \\ \frac{h_{min}^{D-4} - h_{max}^{D-4}}{h_{min}^{D-2} - h_{max}^{D-2}} & \text{if } h \geq \frac{h_{max}}{a} \end{cases} \quad (25)$$

300 Similarly, the main wetting relative effective excess charge density curve  $\hat{Q}_v^{REV,rel,w}$  is  
 301 obtained by replacing Eqs. (10) and (12) into Eq. (23):

$$\hat{Q}_v^{REV,rel,w}(h) = \begin{cases} 1 & \text{if } h \leq h_{min} \\ \frac{h^{D-2} - h_{max}^{D-2}}{h^{D-4} - h_{max}^{D-4}} \cdot \frac{h_{min}^{D-4} - h_{max}^{D-4}}{h_{min}^{D-2} - h_{max}^{D-2}} & \text{if } h_{min} < h < h_{max} \\ \frac{h_{min}^{D-4} - h_{max}^{D-4}}{h_{min}^{D-2} - h_{max}^{D-2}} & \text{if } h \geq h_{max} \end{cases} \quad (26)$$

302 Note that the relative effective excess charge density expressions for both drying and  
 303 wetting have analytical closed form expressions which depend on independent parameters  
 304 ( $a$ ,  $D$ ,  $h_{min}$  and  $h_{max}$ ) with geometrical and physical meaning.

### 305 3 Sensitivity analysis of the model

306 In order to study the role of the model parameters in the estimates of the relative effective  
 307 excess charge density, we perform a parametric analysis of Eqs. (25) and (26). We test  
 308 the influence of the fractal dimension  $D$ , the radial factor  $a$  that controls the pore throats

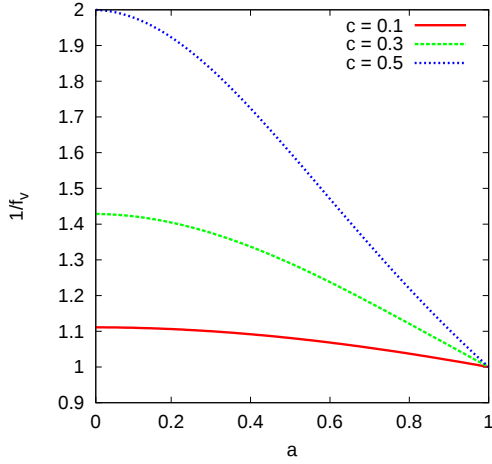


Figure 2: Dimensionless factor  $1/f_v$  as a function of the radial factor  $a$  for different constant values of parameter  $c$ .

309 and the minimum pore size  $R_{min}$  as these parameters produce the greatest impact in the  
 310 size distribution and geometry of the porous media. The following reference values of  
 311 these parameters are considered:  $D = 1.5$ ,  $a = 0.5$  and  $R_{min} = 1.5 \times 10^{-4}$ mm.

312 Figure 3 summarizes this analysis and shows the curves of the hydraulic properties  $S_e$   
 313 and  $k_{rel}$  (Eqs. (8), (10), (11) and (12)) besides the relative effective excess charge density  
 314 curves (Eqs. (25) and (26)). Figures 3a-c show the effect of the fractal dimension for fixed  
 315 values of the other parameters. It can be observed that parameter  $D$  produces significant  
 316 differences between the hysteretic loops of the effective saturation curves, while it slightly  
 317 affects the loops of the relative permeability. For high pressure head values, no significant  
 318 variations are shown among the  $S_e$  and  $k_{rel}$  curves, nevertheless, the asymptotic values  
 319 of the relative effective excess charge density vary with the different values of parameter  
 320  $D$  (see Fig. 3c). In fact, note that the maximum value of  $\hat{Q}_v^{REV,rel}$  increases when  $D$   
 321 decreases, however, this variation remains within one order of magnitude. Figures 3d-f  
 322 show the effect of the radial factor  $a$ . The influence of this parameter is significant in the  
 323 main drying curves of effective saturation and relative permeability for the entire range  
 324 of pressure head values. However, no variations are observed in the main wetting curves  
 325 of the hydraulic properties since they are independent of  $a$ , and hence these curves are  
 326 overlapping each other for the different values of  $a$ . As a result, this parameter strongly  
 327 affects only the main drying  $\hat{Q}_v^{REV,rel}$  curve for all the pressure head values. Indeed, the  
 328 hysteresis cycle for  $\hat{Q}_v^{REV,rel}$  increases for low values of  $a$  since the increasing distance  
 329 between the curves of the drainage and imbibition experiments (see Fig. 3f). As  $a$   
 330 tends toward 1, the two main  $\hat{Q}_v^{REV,rel}$  curves tend to reduce their distance, as it can be  
 331 expected since this limit case represents a tube of constant radius and thus no hysteretic  
 332 phenomenon will be observed. Figures 3g-i show the effect of  $R_{min}$ , this parameter is  
 333 inversely proportional to  $h_{max}$  (Eq. (7)). The effect of  $R_{min}$  is significant in the  $S_e$   
 334 hysteretic loops for increasing values of pressure head, while it is not significant in the  
 335  $k_{rel}$  curves. Hence, the  $\hat{Q}_v^{REV,rel}$  curves show the strongest differences for high values of

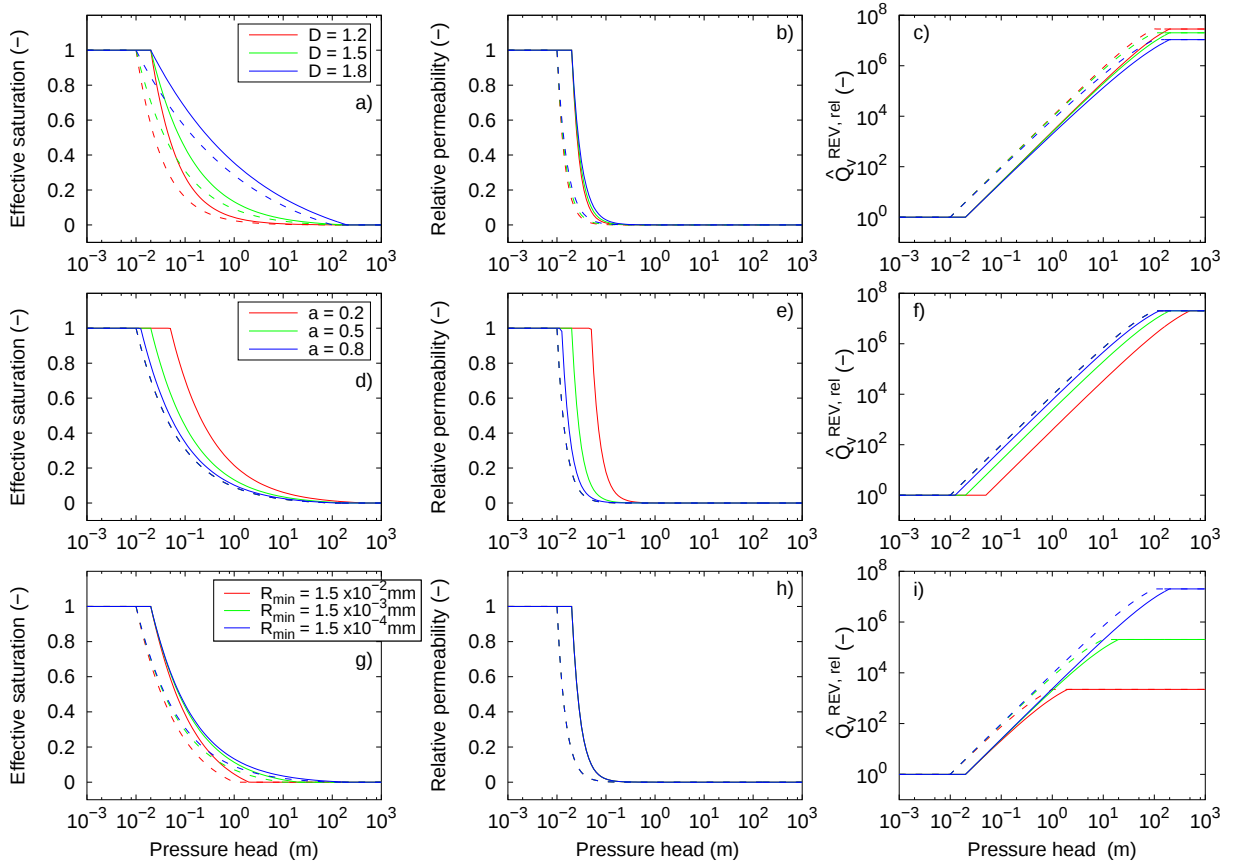


Figure 3: Parametric analysis of the relative effective excess charge density  $\hat{Q}_v^{REV,rel}$  for drainage (solid lines) and imbibition (dashed lines): c) sensitivity to the fractal dimension  $D$ , f) sensitivity to the radial factor  $a$ , and i) sensitivity to the minimum radius  $R_{min}$  (which corresponds to values of  $h_{max}$ , see Eq. (7)). Note that fixed values of the remaining parameters were considered in each case. The corresponding curves of effective saturation (Fig.3(a), 3(d) and 3(g)) and relative permeability (Fig.3(b), 3(e) and 3(h)) are also shown.

336 pressure head. It can also be observed that the maximum value of  $\hat{Q}_v^{REV,rel}$  increases  
 337 when  $R_{min}$  decreases (see Fig. 3i) since, at residual water saturation, the pores with  
 338 smaller radius are the ones that remain with water and a significant amount of excess  
 339 charge is dragged. In addition, note that this parameter can change  $\hat{Q}_v^{REV,rel}$  in 3 orders  
 340 of magnitude while the distance between the main drying and wetting curves of the loops  
 341 remains approximately constant.

342 Finally, from this parametric analysis, we can conclude that parameters  $a$  and  $R_{min}$   
 343 produce the most significant changes in the estimates of  $\hat{Q}_v^{REV,rel}$ . Furthermore, while the  
 344 estimates of the main drying  $\hat{Q}_v^{REV,rel}$  curve are highly sensitive to parameter  $a$  which  
 345 produces strong differences between this curve and the wetting  $\hat{Q}_v^{REV,rel}$  curve, parameter  
 346  $R_{min}$  can modify  $\hat{Q}_v^{REV,rel}$  values over several orders of magnitude.

## 4 Relative coupling coefficient

The effective excess charge is an efficient parameter to study the electrokinetic coupling under partially saturated conditions. This parameter is the basis of an approach that has been increasingly employed in the last decades, nevertheless, the Helmholtz-Smoluchowski approach is the most used in the literature which is based on the coupling coefficient  $C_{EK}$ . This coefficient relates an electrical potential difference and a hydraulic pressure head difference generated by the water flow. The relationship between the relative coupling coefficient  $C_{EK}^{rel}$  and the relative effective excess charge density  $\hat{Q}_v^{REV,rel}$  can be obtained from Eq. (1) (e.g. Linde et al., 2007; Revil et al., 2007):

$$C_{EK}^{rel,i} = \frac{\hat{Q}_v^{REV,rel,i} k_{rel}^i}{\sigma^{rel}}, \quad (27)$$

where Eqs. (11) and (19) are used to calculate this parameter for the drainage case, and Eqs. (12) and (20) for the imbibition case, whereas the relative electrical conductivity is estimated using Archie's second law (Archie et al., 1942),  $\sigma^{rel} = S_w^n$  being  $n$  the water saturation exponent. In this sensitivity analysis, we consider a simple non-hysteretic model for the electrical conductivity to better focus on the hysteresis in the effective excess charge density function. We then considered two different soil textures to study the estimates and behaviour of the coupling parameter within the framework of the approach based on the effective excess charge and the Helmholtz-Smoluchowski approach. The soil textures are a sand and a silt which were used by Soldi et al. (2017) to estimate the hysteretic saturation from the experimental data from Pham et al. (2003). Table 1 lists the parameters used to estimate the hydraulic and electrical properties of the two textures. The hydraulic parameters were taken from Soldi et al. (2017) for both textures, while the electrical parameter was taken from Lesmes and Friedman (2005) and Doussan and Ruy (2009) for the sand and silt respectively.

Fig. 4 shows the relative effective excess charge density  $\hat{Q}_v^{REV,rel}$  and the relative coupling coefficient  $C_{EK}^{rel}$  as functions of both the pressure head  $h$  and effective water saturation  $S_e$  for the two different soil textures. It is interesting to note that the hysteretic effect on both  $\hat{Q}_v^{REV,rel}$  and  $C_{EK}^{rel}$  can be observed when these parameters vary with pressure head values (see Figs. 4a and 4c). However, when they are represented as a function of  $S_e$ , the resulting curve is non-hysteretic as shown in Figs. 4b and 4d. For a fixed value of pressure head, the estimates of  $\hat{Q}_v^{REV,rel}$  vary significantly between the two soil textures (being the greater values for the sand) while the differences in the estimates of  $C_{EK}^{rel}$  are smaller between the two textures. It can also be observed that whereas the  $\hat{Q}_v^{REV,rel}$  values vary over several orders of magnitude (about 2 and 6 orders for the silt and the sand, respectively), the  $C_{EK}^{rel}$  values remain within the range 0~1.1 for the two soil textures. For all the effective saturation range, the  $C_{EK}^{rel}$  curve for the silt remains below the corresponding curve for the sand. Nevertheless, the estimates of  $\hat{Q}_v^{REV,rel}$  for the silt are smaller than the estimates for the sand only for low saturation values.

In a recent study, Zhang et al. (2017) proposed a model to determine the saturation dependence of the relative coupling coefficient and observed from that relationship that

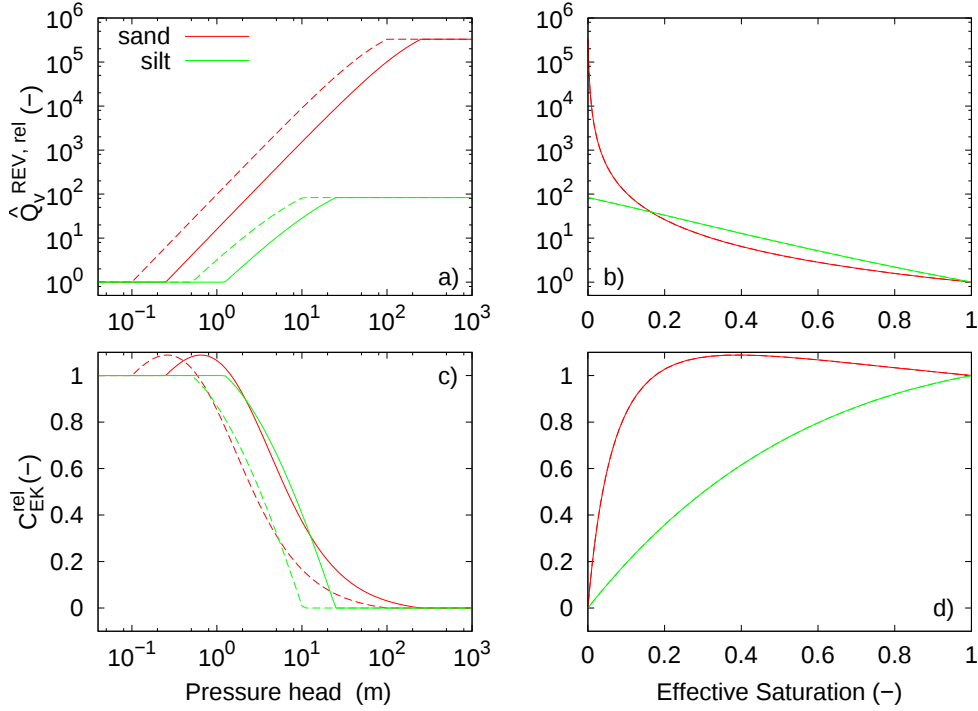


Figure 4: (a,b) Relative effective excess charge density and (c,d) relative coupling coefficient as functions of pressure head and effective saturation for two soil textures: a sand and a silt. The solid and dashed lines in Figs.4(a) and 4(c) correspond to the drainage and imbibition cases, respectively.

386  $C_{EK}^{rel}$  exhibits hysteresis. Such behaviour can not be explained by the model developed  
387 in this study as the resulting  $C_{EK}^{rel}-S_e$  curve is non-hysteretic. The hysteresis observed by  
388 Zhang et al. (2017) could be attributed to the numerical approximations used to calculate  
389 water saturation or other phenomena such as changes in wettability or entrapped air.  
390 From a theoretical point of view, no hysteresis phenomenon is present in  $C_{EK}^{rel}$  when  
391 expressed as a function of effective saturation. Note that the behaviour of the proposed  
392  $C_{EK}^{rel}-S_e$  curves, shown in Fig. 4d, is consistent with previous works considering the  
393 coupling coefficient (e.g., Bordes et al., 2015) and theoretical models assuming the porous  
394 media as bundles of capillary tubes (see Figs. 6c and 6d from Jougnot et al., 2012). The  
395 model of Jackson (2010) predicted a decrease in the estimates of  $C_{EK}^{rel}$  when decreasing  
396  $S_e$ . In addition, the model derived by Jougnot et al. (2012) also predicted that the  $C_{EK}^{rel}$   
397 values decrease when  $S_e$  decreases. Moreover, they observed strong differences on the  
398  $\hat{Q}_v^{REV,rel}$  and  $C_{EK}^{rel}$  estimates as functions of  $S_e$  for different soil textures (see their Fig. 6).  
399 They also showed that  $C_{EK}^{rel}$  can reach values greater than 1 for low effective saturation  
400 values when considering a sand texture, but that it remains smaller than 1 for a silt. As  
401 shown in Fig. 4d, this behaviour of  $C_{EK}^{rel}$  for those two textures is also predicted by the  
402 proposed model.

Table 1: Values of the parameters used to estimate the relative effective excess charge density and the relative coupling coefficient for a sand and a silt.

Soil type	Proposed model parameters*				Electrical parameter <sup>+</sup>
	$D$ (-)	$a$ (-)	$h_{min}$ (m)	$h_{max}$ (m)	$n$ (-)
Sand	1.02	0.40	0.112	100.00	1.30
Silt	1.76	0.41	0.510	10.20	5.96

\*Values taken from Soldi et al. (2017).

<sup>+</sup>The sand value was taken from Lesmes and Friedman (2005), while the silt value from Doussan and Ruy (2009).

## 5 Comparison with experimental data

Data sets of coupling coefficient-pressure head for drainage and imbibition experiments are lacking thus far in the literature. Allègre et al. (2014) studied the self-potential (SP) response to a periodic succession of drainage and imbibition cycles in a column filled with clean Fontainebleau sand. They measured values of pressure head  $h$  at two different points ( $h_1$  and  $h_2$ ) of the column and the SP differences  $\Delta V$  between them. In order to test the proposed model, we estimated relative coupling coefficient values  $C_{EK}^{rel}$  from the recorded data (see Fig. 4 from Allègre et al., 2014) as a function of the mean pressure head value between the two points as follows:

$$C_{EK}^{rel} \left( h_1 + \frac{\Delta h}{2} \right) = \frac{1}{C_{EK}^{sat}} \frac{\Delta V}{\Delta h}, \quad (28)$$

where  $\Delta h = h_2 - h_1$  corresponds to the pressure head differences between the points. For  $C_{EK}^{sat}$ , we considered the value measured by Allègre et al. (2014) for the sand column under total saturation conditions.

Figure 5 shows the  $C_{EK}^{rel}$  data obtained from Allègre et al. (2014) using Eq. (28) and the relative coupling coefficient model for the sand estimated previously in Section 4. The data show high scattering, nevertheless, it can be observed that the behaviour shown by the  $C_{EK}^{rel}$  data values is different for the drainage and for the imbibition experiments. Even so, it is not possible to establish a clear pattern of the data in either of the cases. Note also that the  $C_{EK}^{rel}$  values of the experimental data reach values greater than 1 as predicted by the proposed model.

## 6 Discussion and conclusion

A physically based theoretical model to describe hysteresis phenomenon in the estimates of the effective excess charge density for partially saturated conditions has been presented.



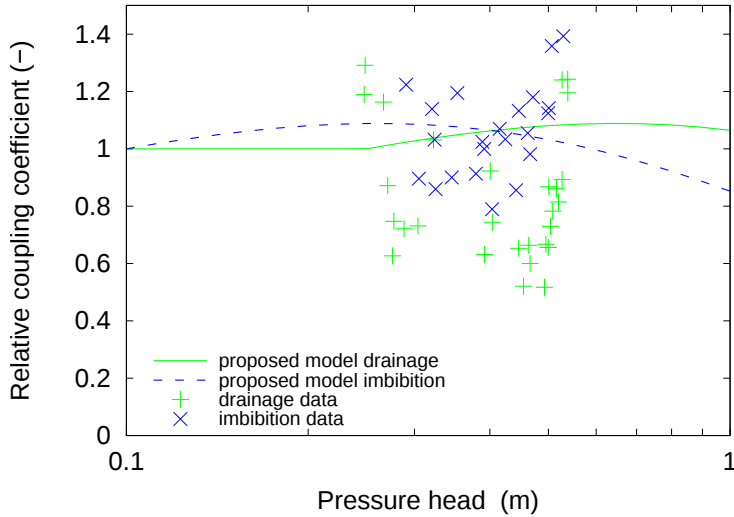


Figure 5: Relative coupling coefficient as a function of pressure head for experimental data from a sand sample from Allègre et al. (2014).

425 The proposed model is based on the assumption that the porous medium can be repre-  
 426 sented by a bundle of tortuous capillary tubes with periodic pore throats. The derivation  
 427 of the model involved upscaling procedures at pore and REV scales of the hydraulic and  
 428 electrokinetic properties of the porous medium. Considering a fractal distribution of pore  
 429 sizes and a binary symmetric 1:1 electrolyte, analytical closed-form expressions have been  
 430 obtained for the effective excess charge density  $\hat{Q}_v^{REV}$  for the drainage and imbibition  
 431 experiments.

432 The hysteretic behaviour of the effective excess charge density is explicitly observed in  
 433 the relative factor  $\hat{Q}_v^{REV,rel}$  when expressed as a function of pressure head since it depends  
 434 on the flow history of the medium. This phenomenon is easily introduced in the model by  
 435 the presence of the pore throats as it strongly controls the flow properties of the medium.  
 436 The radial factor  $a$  plays a key role to represent the hysteresis in the proposed model as it  
 437 controls the size of the pore throats. In addition, if  $a = 1$  (pores with constant radii), the  
 438 expression of the proposed model becomes the expression proposed by Soldi et al. (2019)  
 439 for non-constrictive tortuous capillaries.

440 The saturated effective excess charge density factor  $\hat{Q}_v^{REV,sat}$  depends on the petro-  
 441 physical properties of the medium and the chemical parameters of the pore water while  
 442 also being affected by the presence of the pore throats through the factor  $f_k/f_v^2$ . This  
 443 factor depends on the radial  $a$  and length  $c$  factors of the pore throat. In the limit case  
 444 of a non-constrictive tube ( $a = 1$ ), the expression of the  $\hat{Q}_v^{REV,sat}$  factor is the equation  
 445 obtained by Soldi et al. (2019) for saturated conditions.

446 The influence of the model parameters ( $D$ ,  $a$  and  $R_{min}$ ) on the estimates of the relative  
 447 effective excess charge density has been tested by a sensitivity analysis. The results  
 448 show that variations of the fractal dimension  $D$  slightly affect the  $\hat{Q}_v^{REV,rel}$  estimates.  
 449 Nevertheless, the effects of the radial factor  $a$  and the minimum pore radius  $R_{min}$  produce

450 the most significant variations in the  $\hat{Q}_v^{REV,rel}$  values. The factor  $a$  controls the shape of  
451 the hysteretic loop (the distance between the drainage and imbibition curves), and in  
452 the limit case of  $a = 1$ , the hysteresis disappears from the  $\hat{Q}_v^{REV,rel}$  curves as it will  
453 be expected. Nonetheless, the variations of  $R_{min}$  can affect the  $\hat{Q}_v^{REV,rel}$  estimates over  
454 several orders of magnitude.

455 The comparison of the relative effective excess charge density and the relative coupling  
456 coefficient estimates for two different soil textures shows that both parameters exhibit the  
457 hysteresis phenomenon when expressed as functions of the pressure head. However, a  
458 non-hysteretic behaviour is observed when they are described as functions of the effective  
459 saturation. The comparison of the two soil textures also shows significant differences in  
460 the estimates of  $\hat{Q}_v^{REV,rel}$ . In fact, it could be observed that its value varies over 6 orders  
461 of magnitude for the sand while over 2 orders for the silt. Nevertheless, the  $C_{EK}^{rel}$  values  
462 vary in a small range (0~1.1 approximately) for both textures.

463 To the best of our knowledge, the data shown in Figure 5 are the only hysteretic  
464 data available to validate coupling coefficient curves as function of pressure head values.  
465 From a qualitative comparison, the  $C_{EK}^{rel}$  values estimated from the proposed model are  
466 consistent with the experimental data values. Even though, further drainage-imbibition  
467 tests are needed, the proposed model provides a simple and physically meaningful way to  
468 include hysteresis effects on the electrokinetic potential.

469 Based on the framework of the effective excess charge, the present study represents a  
470 step forward to understand the electrokinetic coupling under partially saturated condi-  
471 tions since the model includes hysteresis phenomenon in SP signals. As far as reported in  
472 literature, this is the first analytical model that accounts this phenomenon in the stream-  
473 ing potential. Therefore, this simple model can be a valuable starting point to the use of  
474 the SP method in hydrogeophysics studies to non-intrusively monitor unsaturated ground-  
475 water fluxes (e.g., Doussan et al., 2002; Suski et al., 2006; Jougnot et al., 2015; Voytek  
476 et al., 2019; Hu et al., 2020) and help to improve the understanding of processes occurring  
477 in the vadose zone, such as contaminant plumes (e.g. Naudet et al., 2003; Minsley et al.,  
478 2007), hydro-fracturing (e.g. Darnet et al., 2006; Haas et al., 2013) or related to reservoir  
479 engineering (Saunders et al., 2006).

## 480 Acknowledgments

481 This research is partially supported by Universidad Nacional de La Plata, Consejo Na-  
482 cional de Investigaciones Científicas y Técnicas (Argentina), Sorbonne Université and  
483 Centre National de la Recherche Scientifique (France). The authors strongly thank the  
484 Editor and an anonymous reviewer for their constructive comments. D.J. strongly thanks  
485 the financial support of the CNRS INSU EC2CO program for funding the STARTREK  
486 (Système péTrophysique de cAractéRisation du Transport Réactif en miliEu Karstique)  
487 project.

488 authoryear

## References

- 489
- 490 Allègre, V., Maineult, A., Lehmann, F., Lopes, F., Zamora, M., 2014. Self-potential  
491 response to drainage–imbibition cycles. *Geophysical Journal International* 197, 1410–  
492 1424.
- 493 Archie, G.E., et al., 1942. The electrical resistivity log as an aid in determining some  
494 reservoir characteristics. *Transactions of the AIME* 146, 54–62.
- 495 Bear, J., 1998. *Dynamics of fluids in porous media*. Dover Publications, Inc., Mineola,  
496 N.Y.
- 497 Beliaev, A.Y., Hassanizadeh, S., 2001. A theoretical model of hysteresis and dynamic  
498 effects in the capillary relation for two-phase flow in porous media. *Transport in Porous*  
499 *media* 43, 487–510.
- 500 Bordes, C., Sénéchal, P., Barrière, J., Brito, D., Normandin, E., Jougnot, D., 2015. Impact  
501 of water saturation on seismoelectric transfer functions: a laboratory study of coseismic  
502 phenomenon. *Geophysical Journal International* 200, 1317–1335.
- 503 Buckingham, E., 1907. *Studies on the movement of soil moisture*. US Dept. Agric. Bur.  
504 *Soils Bull.* 38.
- 505 Büsing, H., Vogt, C., Ebigbo, A., Klitzsch, N., 2017. Numerical study on co2 leakage  
506 detection using electrical streaming potential data. *Water Resources Research* 53, 455–  
507 469.
- 508 Darcy, H., 1856. *Exposition et application des principes à suivre et des formules à employer*  
509 *dans les questions de distribution d’eau. Les fontaines publiques de la ville de Dijon,*  
510 *Eds. Victor Dalmont, Paris 1856.*
- 511 Darnet, M., Marquis, G., SAILHAC, P., 2006. Hydraulic stimulation of geothermal reservoirs:  
512 fluid flow, electric potential and microseismicity relationships. *Geophysical Journal*  
513 *International* 166, 438–444.
- 514 Doussan, C., Jouniaux, L., Thony, J.L., 2002. Variations of self-potential and unsaturated  
515 water flow with time in sandy loam and clay loam soils. *Journal of Hydrology* 267, 173–  
516 185.
- 517 Doussan, C., Ruy, S., 2009. Prediction of unsaturated soil hydraulic conduc-  
518 tivity with electrical conductivity. *Water Resources Research* 45, W10408,  
519 doi:10.1029/2008WR007309.
- 520 Fan, Y., Grant, G., Anderson, S.P., 2019. Water within, moving through, and shaping the  
521 earth’s surface: Introducing a special issue on water in the critical zone. *Hydrological*  
522 *Processes* , <https://onlinelibrary.wiley.com/doi/abs/10.1002/hyp.13638>.

- 523 Glover, P.W., Déry, N., 2010. Streaming potential coupling coefficient of quartz glass  
524 bead packs: Dependence on grain diameter, pore size, and pore throat radius streaming  
525 potential and grain diameter. *Geophysics* 75, F225–F241.
- 526 Guarracino, L., Jougnot, D., 2018. A physically based analytical model to describe effec-  
527 tive excess charge for streaming potential generation in water saturated porous media.  
528 *Journal of Geophysical Research: Solid Earth* 123, 52–65.
- 529 Guarracino, L., Rötting, T., Carrera, J., 2014. A fractal model to describe the evolution  
530 of multiphase flow properties during mineral dissolution. *Advances in water resources*  
531 67, 78–86.
- 532 Guichet, X., Jouniaux, L., Pozzi, J.P., 2003. Streaming potential of a sand column in  
533 partial saturation conditions. *Journal of Geophysical Research: Solid Earth* 108.
- 534 Haas, A., Revil, A., 2009. Electrical burst signature of pore-scale displacements. *Water*  
535 *Resources Research* 45.
- 536 Haas, A., Revil, A., Karaoulis, M., Frash, L., Hampton, J., Gutierrez, M., Mooney, M.,  
537 2013. Electric potential source localization reveals a borehole leak during hydraulic  
538 fracturing. *Geophysics* 78, D93–113.
- 539 Hu, K., Jougnot, D., Huang, Q., Looms, M.C., Linde, N., 2020. Advancing quantita-  
540 tive understanding of self-potential signatures in the critical zone through long-term  
541 monitoring. *Journal of Hydrology* 585, 124771.
- 542 Hunter, R., 1981. *Zeta potential in colloid science: Principles and applications*. New  
543 York, USA .
- 544 Jackson, M.D., 2008. Characterization of multiphase electrokinetic coupling using a  
545 bundle of capillary tubes model. *Journal of Geophysical Research: Solid Earth* 113,  
546 doi:10.1029/2007JB005490.
- 547 Jackson, M.D., 2010. Multiphase electrokinetic coupling: Insights into the impact of  
548 fluid and charge distribution at the pore scale from a bundle of capillary tubes model.  
549 *Journal of Geophysical Research: Solid Earth* 115, doi:10.1029/2009JB007092.
- 550 Jardani, A., Dupont, J.P., Revil, A., 2006. Self-potential signals associated with prefer-  
551 ential groundwater flow pathways in sinkholes. *Journal of Geophysical Research: Solid*  
552 *Earth* 111, doi:10.1029/2005JB004231.
- 553 Jerauld, G., Salter, S., 1990. The effect of pore-structure on hysteresis in relative per-  
554 meability and capillary pressure: pore-level modeling. *Transport in porous media* 5,  
555 103–151.
- 556 Jougnot, D., Linde, N., 2013. Self-potentials in partially saturated media: the importance  
557 of explicit modeling of electrode effects. *Vadose Zone Journal* 12.

- 558 Jougnot, D., Linde, N., Haarder, E.B., Looms, M.C., 2015. Monitoring of saline tracer  
559 movement with vertically distributed self-potential measurements at the hobe agricul-  
560 tural test site, vouldund, denmark. *Journal of Hydrology* 521, 314–327.
- 561 Jougnot, D., Linde, N., Revil, A., Doussan, C., 2012. Derivation of soil-specific streaming  
562 potential electrical parameters from hydrodynamic characteristics of partially saturated  
563 soils. *Vadose Zone Journal* 11, doi:10.2136/vzj2011.0086.
- 564 Jougnot, D., Mendieta, A., Leroy, P., Mainault, A., 2019. Exploring the effect of the  
565 pore size distribution on the streaming potential generation in saturated porous media,  
566 insight from pore network simulations. *Journal of Geophysical Research: Solid Earth*  
567 124, 5315–5335, <https://doi.org/10.1029/2018JB017240>.
- 568 Jougnot, D., Roubinet, D., Guarracino, L., Mainault, A., 2020. Modeling streaming  
569 potential in porous and fractured media, description and benefits of the effective excess  
570 charge density approach, in: *Advances in Modeling and Interpretation in Near Surface*  
571 *Geophysics*. Springer, pp. 61–96.
- 572 Jury, W., Gardner, W.R., Gardner, W.H., 1991. *Soil physics*, john wiley & sons. Inc.  
573 New York .
- 574 Klausner, Y., 1991. *Fundamentals of Continuum Mechanics of Soils*. Springer, New York.
- 575 Kormiltsev, V.V., Ratushnyak, A.N., Shapiro, V.A., 1998. Three-dimensional modeling  
576 of electric and magnetic fields induced by the fluid flow movement in porous media.  
577 *Physics of the earth and planetary interiors* 105, 109–118.
- 578 Lenhard, R., Parker, J., 1987. A model for hysteretic constitutive relations governing  
579 multiphase flow: 2. permeability-saturation relations. *Water Resources Research* 23,  
580 2197–2206.
- 581 Lesmes, D.P., Friedman, S.P., 2005. Relationships between the electrical and hydroge-  
582 ological properties of rocks and soils, in: *Hydrogeophysics*. Springer, New York, pp.  
583 87–128.
- 584 Linde, N., 2009. Comment on “characterization of multiphase electrokinetic coupling  
585 using a bundle of capillary tubes model” by mathew d. jackson. *Journal of Geophysical*  
586 *Research: Solid Earth* 114, doi:10.1029/2008JB005845.
- 587 Linde, N., Jougnot, D., Revil, A., Matthäi, S., Arora, T., Renard, D., Doussan, C.,  
588 2007. Streaming current generation in two-phase flow conditions. *Geophysical Research*  
589 *Letters* 34, L03306. doi:10.1029/2006GL028878.
- 590 Linde, N., Revil, A., 2007. Inverting self-potential data for redox po-  
591 tentials of contaminant plumes. *Geophysical Research Letters* 34, L14302.  
592 <https://doi.org/10.1029/2007GL030084>.

- 593 Maineult, A., Strobach, E., Renner, J., 2008. Self-potential signals induced by  
594 periodic pumping tests. *Journal of Geophysical Research: Solid Earth* 113,  
595 doi:10.1029/2007JB005193.
- 596 Malama, B., Kuhlman, K.L., Revil, A., 2009a. Theory of transient streaming poten-  
597 tials associated with axial-symmetric flow in unconfined aquifers. *Geophysical Journal*  
598 *International* 179, 990–1003.
- 599 Malama, B., Revil, A., Kuhlman, K., 2009b. A semi-analytical solution for transient  
600 streaming potentials associated with confined aquifer pumping tests. *Geophysical Jour-*  
601 *nal International* 176, 1007–1016.
- 602 Minsley, B.J., Sogade, J., Morgan, F.D., 2007. Three-dimensional self-potential inversion  
603 for subsurface dnapl contaminant detection at the savannah river site, south carolina.  
604 *Water Resources Research* 43. doi:10.1029/2005WR003996.
- 605 Morgan, F., Williams, E., Madden, T., 1989. Streaming potential properties of westerly  
606 granite with applications. *Journal of Geophysical Research: Solid Earth* 94, 12449–  
607 12461.
- 608 Mualem, Y., 1977. Extension of the similarity hypothesis used for modeling the soil water  
609 characteristics. *Water Resources Research* 13, 773–780.
- 610 Mualem, Y., 1986. Hydraulic conductivity of unsaturated soils: prediction and formulas.  
611 *Methods of Soil Analysis: Part 1—Physical and Mineralogical Methods* , 799–823.
- 612 Naudet, V., Revil, A., Bottero, J.Y., Bégassat, P., 2003. Relationship between self-  
613 potential (sp) signals and redox conditions in contaminated groundwater. *Geophysical*  
614 *research letters* 30. doi:10.1029/2003GL018096.
- 615 Parker, J., Lenhard, R., 1987. A model for hysteretic constitutive relations governing  
616 multiphase flow: 1. saturation-pressure relations. *Water Resources Research* 23, 2187–  
617 2196.
- 618 Petiau, G., 2000. Second generation of lead-lead chloride electrodes for geophysical ap-  
619 plications. *Pure and applied geophysics* 157, 357–382.
- 620 Pham, H., Fredlund, D., Barbour, S., 2003. A practical hysteresis model for the soil-water  
621 characteristic curve for soils with negligible volume change. *Geotechnique* 53, 293–298.
- 622 Pham, H.Q., Fredlund, D.G., Barbour, S.L., 2005. A study of hysteresis models for  
623 soil-water characteristic curves. *Canadian Geotechnical Journal* 42, 1548–1568.
- 624 Revil, A., 2017. Transport of water and ions in partially water-saturated porous  
625 media. part 1. constitutive equations. *Advances in water resources* 103, 119–138,  
626 <https://doi.org/10.1016/j.advwatres.2016.02.006>.

- 627 Revil, A., Gevaudan, C., Lu, N., Maineult, A., 2008. Hysteresis of the self-potential  
628 response associated with harmonic pumping tests. *Geophysical Research Letters* 35,  
629 doi:10.1029/2008GL035025.
- 630 Revil, A., Linde, N., Cerepi, A., Jougnot, D., Matthäi, S., Finsterle, S., 2007. Electroki-  
631 netic coupling in unsaturated porous media. *Journal of colloid and interface science*  
632 313, 315–327.
- 633 Revil, A., Schwaeger, H., Cathles, L., Manhardt, P., 1999. Streaming potential in porous  
634 media: 2. theory and application to geothermal systems. *Journal of Geophysical Re-*  
635 *search: Solid Earth* 104, 20033–20048.
- 636 Rizzo, E., Suski, B., Revil, A., Straface, S., Troisi, S., 2004. Self-potential signals asso-  
637 ciated with pumping tests experiments. *Journal of Geophysical Research: Solid Earth*  
638 109, doi:10.1029/2004JB003049.
- 639 Saunders, J., Jackson, M., Pain, C., 2006. A new numerical model of electrokinetic  
640 potential response during hydrocarbon recovery. *Geophysical research letters* 33.  
641 doi:10.1029/2006GL026835.
- 642 Sill, W.R., 1983. Self-potential modeling from primary flows. *Geophysics* 48, 76–86.
- 643 Solazzi, S.G., Guarracino, L., Rubino, J.G., Holliger, K., 2019. Saturation hys-  
644 teresis effects on the seismic signatures of partially saturated heterogeneous porous  
645 rocks. *Journal of Geophysical Research: Solid Earth* Accepted for publication,  
646 <https://doi.org/10.1029/2019JB017726>.
- 647 Soldi, M., Guarracino, L., Jougnot, D., 2017. A simple hysteretic constitutive model for  
648 unsaturated flow. *Transport in Porous Media* 120, 271–285.
- 649 Soldi, M., Jougnot, D., Guarracino, L., 2019. An analytical effective excess charge density  
650 model to predict the streaming potential generated by unsaturated flow. *Geophysical*  
651 *Journal International* 216, 380–394.
- 652 Soueid Ahmed, A., Jardani, A., Revil, A., Dupont, J.P., 2014. Hydraulic conductivity  
653 field characterization from the joint inversion of hydraulic heads and self-potential data.  
654 *Water Resources Research* 50, 3502–3522.
- 655 Soueid Ahmed, A., Jardani, A., Revil, A., Dupont, J.P., 2016. Joint inversion of hydraulic  
656 head and self-potential data associated with harmonic pumping tests. *Water Resources*  
657 *Research* 52, 6769–6791.
- 658 Stern, O., 1924. Zur theorie der elektrolytischen doppelschicht. *Zeitschrift für Elektro-*  
659 *chemie und angewandte physikalische Chemie* 30, 508–516.
- 660 Straface, S., Fallico, C., Troisi, S., Rizzo, E., Revil, A., 2007. An inverse procedure to  
661 estimate transmissivity from heads and sp signals. *Groundwater* 45, 420–428.

- 662 Suski, B., Revil, A., Titov, K., Konosavsky, P., Voltz, M., Dages, C., Huttel, O., 2006.  
663 Monitoring of an infiltration experiment using the self-potential method. *Water Re-*  
664 *sources Research* 42. doi:10.1029/2005WR004840.
- 665 Thanh, L.D., Jougnot, D., Van Do, P., Van Nghia A, N., 2019. A physically based model  
666 for the electrical conductivity of water-saturated porous media. *Geophysical Journal*  
667 *International* 219, 866–876.
- 668 Thanh, L.D., Van Do, P., Van Nghia, N., Ca, N.X., 2018. A fractal model for streaming  
669 potential coefficient in porous media. *Geophysical Prospecting* 66, 753–766.
- 670 Topp, G., 1971. Soil-water hysteresis: the domain theory extended to pore interaction  
671 conditions 1. *Soil Science Society of America Journal* 35, 219–225.
- 672 Topp, G.C., Miller, E., 1966. Hysteretic moisture characteristics and hydraulic conduc-  
673 tivities for glass-bead media1. *Soil Science Society of America Journal* 30, 156–162.
- 674 Tyler, S.W., Wheatcraft, S.W., 1990. Fractal processes in soil water retention. *Water*  
675 *Resources Research* 26, 1047–1054.
- 676 Van Genuchten, M.T., 1980. A closed-form equation for predicting the hydraulic conduc-  
677 tivity of unsaturated soils. *Soil Sci. Soc. Am. J* 44, 892–898.
- 678 Vogel, H.J., Roth, K., 2001. Quantitative morphology and network representation of soil  
679 pore structure. *Advances in water resources* 24, 233–242.
- 680 Voytek, E.B., Barnard, H.R., Jougnot, D., Singha, K., 2019. Transpiration- and  
681 precipitation-induced subsurface water flow observed using the self-potential method.  
682 *Hydrological Processes* 33, 1784–1801, <https://doi.org/10.1002/hyp.13453>.
- 683 Wang, S., Wu, T., Qi, H., Zheng, Q., Zheng, Q., 2015. A permeability model  
684 for power-law fluids in fractal porous media composed of arbitrary cross-section  
685 capillaries. *Physica A: Statistical Mechanics and its Applications* 437, 12–20,  
686 <https://doi.org/10.1016/j.physa.2015.05.089>.
- 687 Waxman, M., Smits, L., 1968. Electrical conductivities in oil-bearing shaly sands. *Society*  
688 *of Petroleum Engineers Journal* 8, 107–122.
- 689 Xu, C., Torres-Verdín, C., 2013. Pore system characterization and petrophysical rock  
690 classification using a bimodal gaussian density function. *Mathematical Geosciences* 45,  
691 753–771.
- 692 Yu, B., Li, J., Li, Z., Zou, M., 2003. Permeabilities of unsaturated fractal porous media.  
693 *International journal of multiphase flow* 29, 1625–1642.
- 694 Zhang, J., Vinogradov, J., Leinov, E., Jackson, M., 2017. Streaming potential during  
695 drainage and imbibition. *Journal of Geophysical Research: Solid Earth* .